River ice phenology and thickness from satellite altimetry: Potential for ice bridge road operation

Elena Zakharova[1,2], Svetlana Agafonova[3], Claude Duguay[4,5], Natalia Frolova[3], Alexei Kouraev[6]

1. Institute of Water Problems of Russian Academy of Science, Moscow, Russia,

2. EOLA, Toulouse, France

3. Moscow State University, Moscow, Russia,

4. University of Waterloo, Waterloo, Canada

5. H2O Geomatics, Waterloo, Canada

6. LEGOS, Université de Toulouse, CNES, CNRS, IRD, UPS Toulouse, France

Abstract

River ice is an important component of the cryosphere. Satellite monitoring of river ice is a rapidly developing area of scientific research which has potential for many climate, environmental, and socio-economic applications. Radar altimetry, which is widely used for monitoring of river water regimes, demonstrates good potential for the observation of river ice phenology and for the estimation of river ice thickness. Using Jason-2 and -3 Ku-band backscatter measurements we retrieved river ice phenology dates and thickness and found that the altimetric measurements and our algorithm are sensitive enough to detect the first appearance of ice and the beginning of thermal ice degradation on the Lower Ob River (Western Siberia). The uncertainties in ice event timing using altimetry are within 10 days of the satellite repeat cycle for 88–90% of cases. River ice thickness retrieved from altimetric measurements via empirical relations with in-situ observations has an accuracy (expressed as RMSE) varying from 0.07 to 0.18 m. One of the novel potential applications of radar altimetry is the prediction of ice bridge road operations. We demonstrate that using satellite altimetry, the dates of ice road opening in Salekhard City can be predicted with 4 days leading time. Uncertainties for the prediction of dates of ice road closure are three days, with the lead time varying from 4 days (for late melting start) to 22 days (for yearly melting start).

1 Introduction

River ice is a major component of the global cryosphere and hydrosphere, and its monitoring is important for many environmental, climate, and societal applications. River ice plays a key role in the functioning of aquatic and riparian ecosystems (Prowse, 2001). River ice contributes to the erosion of channels and banks (Ettema, 2002) and to the transport of sediments (Beltaos et al., 2018). Ice alters the exchanges of energy and water with the atmosphere (Kourzeneva, 2014) and is responsive to regional climate variability, thus acting as a good indicator of hydro-climate changes (Prowse et al., 2011a). River ice affects streamflow via the withdrawal (immobilisation) of part of the water during freeze-up and consequent release during break-up. In addition, ice jams can cause catastrophic flooding (Beltaos et al., 2013).

Field measurements and satellite estimates of river discharge during the ice/water transition (and vice versa) are not easy tasks (Morse and Hicks, 2005). Consequently, streamflow measurements or discharge estimations during these periods are characterised by high uncertainty (Zakharova et al., 2019). River ice affects the operation of hydropower stations, as well as construction and navigation activities. In arctic regions, frozen rivers provide a unique transportation infrastructure for the movement of merchandise and people via winter ice roads. The presence of river

ice cover also provides local populations with access to fishing grounds and in some cases (e.g. Central Yakutia, Russia) to fresh water.

However, operational monitoring of ice in northern rivers is difficult because of low site accessibility. Moreover, icy conditions can be unsafe for people who are required to perform in-situ measurements, especially at the beginning or end of the ice season. Therefore, satellite remote sensing observation has been proposed as an alternative, or complement, to ground measurements, allowing for the characterisation of river ice at a temporal resolution suitable for addressing various climatic, scientific, and operational requirements.

Satellite-borne instruments provide observational capabilities for many river ice parameters. Optical sensors such as the Moderate Resolution Imaging Spectroradiometer (MODIS) and the Advanced Very High Resolution Radiometer (AVHRR) have been used to map river ice extent and phenology - freeze-up and breakup dates (Pavelsky and Smith, 2004; Chaouch et al., 2014; Chu and Lindenschmidt, 2016; Muhammad et al., 2016; Cooley and Pavelsky, 2016; Beaton et al., 2019). However, the presence of extensive cloud cover for many months of the year and low solar illumination conditions, particularly during the freeze-up period, are limiting factors for ice monitoring of rivers at high latitudes. Active sensors operating in the microwave spectrum are weather independent and provide a spatial resolution higher than that of the MODIS and AVHRR instruments. One such sensor is synthetic aperture radar (SAR), a microwave sensor which has been used to monitor river ice phenology (Unterschultz et al., 2009; Mermoz et al., 2009), deformation (Unterschultz et al., 2009), and classification of ice types (Chu and Lindenschmidt, 2016).

Ice thickness is another parameter which is of particular interest for operational purposes, such as public safety, ice road service, jam forecasts, and mitigation. Passive microwave and thermal satellite instruments for the retrieval of ice thickness have demonstrated capability for large lakes (Kang et al., 2014; Duguay et al., 2002, 2015; Gunn et al., 2015; Kheyrollah Pour et al., 2017). However, the spatial dimension of rivers, notably the width of channels, limits the application of these instruments as they only provide coarse spatial resolution (km to tens of km). Several studies have used active microwave SAR images with high spatial resolution to retrieve river ice thickness (Unterschultz et al., 2009; Mermoz et al., 2014). Altimetric radars are also high resolution weather-independent instruments with a long history of observations starting in the middle of 1980s. Their measurements have been largely used for monitoring the hydrological regime of inland waterbodies and water courses starting at 100 m in width (Michailovsky et al., 2012). Altimetric radars have proven capability in providing measurements for the retrieving of freshwater ice thickness of large Arctic lakes (Beckers et al., 2017). However, in this paper, we demonstrate the application of radar altimetry for monitoring river ice phenology and retrieval of river ice thickness.

The objective of the present study is to investigate the capacity of radar altimetry satellites for retrieving river ice onset/melting dates and ice thickness, as well as providing local communities with operational information useful for ice bridge road construction and maintenance. Two altimetric satellite missions, Jason2 and Jason 3, were selected for this study for two reasons: 1) their best among altimetric missions temporal resolution (10 days); and 2) the long lifetime of this series of satellites providing observations on the same orbit, starting in 1992 with the Topex/Poseidon and continuing nowadays with the Sentinel-6 (on orbit since November 2020).

2 Regional setup and Data

2.1 Study Region

The study was conducted for the Ob River (Siberia, Russia). The Ob River drains the Western Siberian Plain and is the third largest river in the Arctic Ocean watershed, with an annual flow of 406 km^3 (Zakharova et al., 2020). The lower reach of the Ob River extends approximately 800 km and begins from a confluence with the Irtysh River at 61.08°N. This reach is characterised by a particularly wide floodplain (up to 50 km) and the presence of numerous branches. The easternmost channel is the main, largest branch, called the Big Ob. The second largest branch delineates the flood plain from the west (Figure 1). The Ob River watershed is one of the largest peat bog systems in the world (Zakharova et al., 2014), and many settlements, which are located on the high terraces of the two main branches, have limited interconnection and access to supplies. The main branches are navigable; however, they are covered by ice for seven months of the year. In winter, when the bogs freeze, local communities intensify their socio-economic activities by constructing winter roads and ice bridges over river crossings. River ice observations are sparse and are taken only at a few gauging stations dedicated to water level monitoring. For this study, we selected a section of the lower reaches of the Ob River located between two large administrative centres in the region (Salekhard and Khanty-Mansyisk).

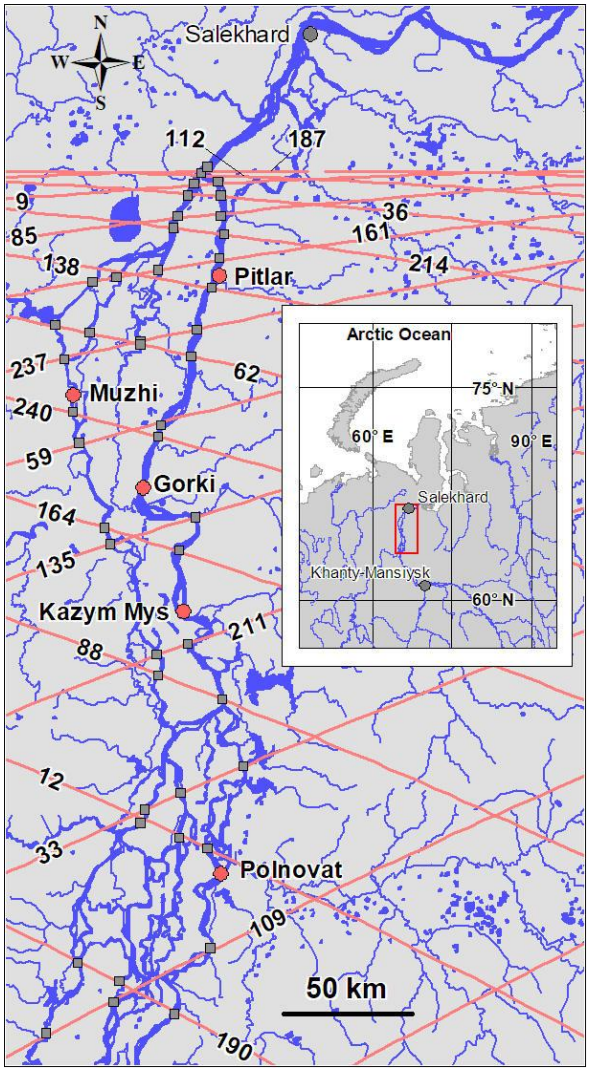

Figure 1: The lower reaches of the Ob River and location of the virtual (grey rectangles) and gauging (red circles) stations. The virtual stations correspond to satellite-river cross-overs. Jason-2 and 3 satellite tracks and corresponding track numbers are also shown. The main map is produced using public The World Bank data (https://datacatalog.worldbank.org/dataset/major-rivers-world).

2.2 Data

2.2.1 In-situ data

The Russian Hydrometeorological Service monitors ice at all gauging stations water level measurements. There are five water level gauging stations in the studied Ob River reach (Figure 1, Table 1). Four stations (Polnovat, Gorki, Kazym-Mys, and Pitlar) are located on the main branch of the Ob River, and one station (Muzhi) provides observations on the secondary channel called the Small Ob River.

Table 1: Gauging stations located in the lower Ob reach.

River- station	Distance from mouth (km)	Beginning of observations	Long observation gaps
Ob – Polnovat	702	1970	
Ob – Gorki	487	1935	
Small Ob – Muzhi	463	1933	
Ob – Kazym Mys	551	1979	1988 –2003
Ob – Pitlar	386	1979	1990 – 2005

The standard protocol of river ice monitoring includes: 1) daily visual observations of ice presence/absence and ice type/events; and 2) 3-6 times per month measurements of ice thickness and on-ice snow depth. Ice thickness was measured by drilling one hole in ice using an ice auger. The snow depth corresponds to the average value calculated from three snow-depth measurements located around the hole.

According to in-situ observations at the gauging stations, ice formation in the study region begins on average between 23-27 October. The earliest and latest records for the last 20 years were 1 October and 18 November, respectively. Ice cover forms quickly on this section of the river, typically within just 2-3 days from appearance first ice. However, in 15% of cases (for the last 20 years), the installation of ice cover can take up to 10 days. Ice develops rapidly during the first month of the ice season and river ice reaches a thickness of 0.23-0.30 m already by the end of November. By the end of the ice growth period (March-April), river ice thickness is 0.80-1.0 m on average (1.50 m maximum value). Snow depth on the ice surface varies from 0.09-0.13 m in November to 0.30-0.50 m in April.

According to observations on the gauging stations the temporal dynamics of ice growth on the large linear channel sections is similar throughout the studied reaches (Fig. 2a). However, in the south of the region, the ice thickness is 0.07-0.20 m less than in the north. Climate change has affected river ice in the Canadian Arctic (Prowse et al., 2011b) and the European part of Russia (Agafonova and Vasilenko, 2020) but has not yet resulted in a significant change in the ice regime in the lower Ob River. No significant long-term trends for ice onset and melt, as well as for maximum ice thickness, were observed at gauging stations in the study region (Figure 2b).

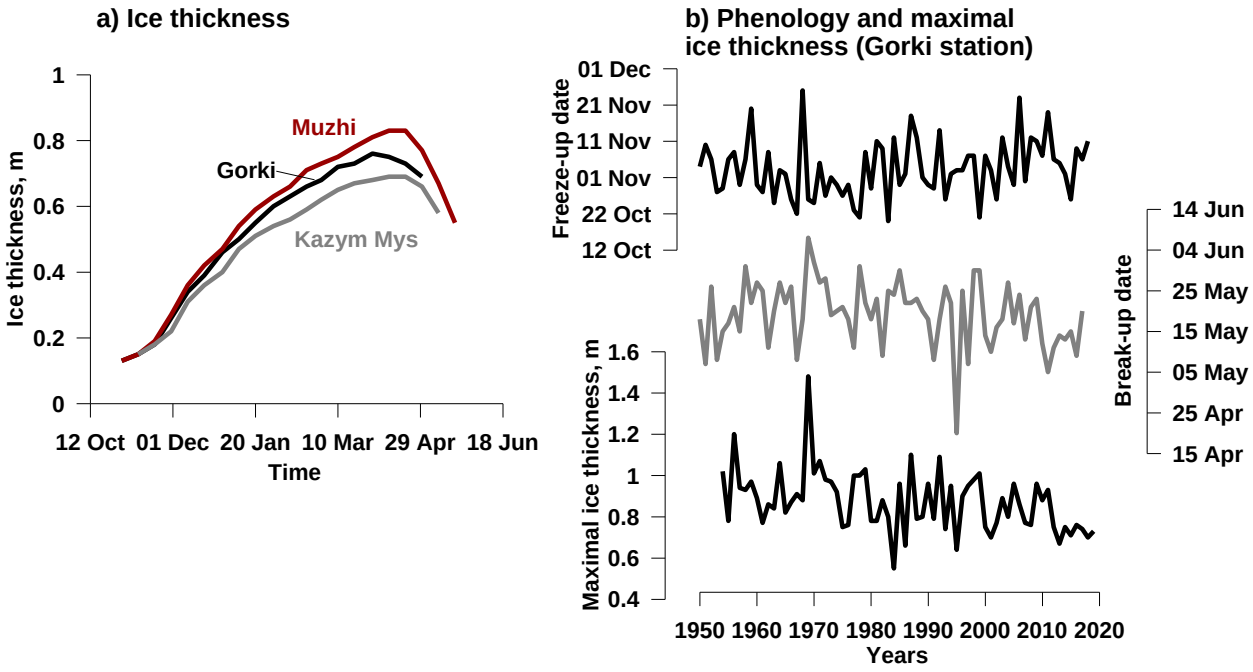

Figure 2: Examples of a) ice thickness seasonal evolution (average values for 1980-2017) at three stations (Gorki, Muzhi and Kazym Mys) along the studied river reaches, and b) temporal dynamic of ice freeze-up, break-up and maximum ice thickness for station Gorki.

2.2.2 Altimetry data

The Jason-2 satellite is the third altimetric satellite of the Topex/Poseidon-Jason series. The satellite operated between 2008-2016 and acquired data in a 10-day repeat orbit with an inclination of 66.08°. One satellite cycle consisted of 127 revolutions and 254 tracks (odd numbers for ascending and even numbers for descending orbits). The altimetric radar aboard Jason-2 provided along-track measurements at Ku (13.6 GHz) and C (5.3 GHz) bands with a sampling frequency of 20 Hz, allowing for a 375 m distance between adjacent radar measurements. The ground track repeatability of the mission was maintained within a ±1 km cross-track at the equator. At the latitudes of our study region (63-66°N), the cross-track oscillation band was approximately 400 m wide. Because the radar ground footprint in the Ku-band is lower than that in the C-band, the measurements in the Ku-band were used in this study. The theoretical footprint of the radar at the Ku-band is 10-12 km in diameter over the rough ocean surface. However, this diameter decreases over smooth inland water and ice surfaces such that the main return signal can come from footprints of just a few kilometres in diameter (Legresy et al., 1998).

The satellite payload of Jason-2 also included a nadir-looking Advanced Microwave Radiometer (AMR), which provides measurements of brightness temperature in 18.7, 23.8, and 34.0 GHz bands at a nadir-looking angle with a sampling frequency of 1 Hz. Brightness temperature measurements acquired with other passive microwave radiometers, such as AMSR-E, have demonstrated good performance for the retrieval of ice thickness on large Great Slave Lake and Great Bear Lake, Canada (Kang et al., 2014). Because the Jason AMR footprints are large, at 42 km (18.7 GHz), 35 km (23.8 GHz), and 22 km (34.0 GHz) in diameter (Kouraev et al., 2007), the radiometric measurements over rivers are dominated by signals emitted mainly from land surfaces surrounding the river channels. In this study, we used Jason-2 and 3 AMR measurements only as auxiliary information to develop additional criteria for adjustment of the radar freezing/melting date retrieval algorithm.

In 2016, the successor to the Jason-2 satellite, the Jason-3, was sent into space with the same orbit and instruments as Jason-2. For 20 cycles, the two missions flew with an 80-second time lag, ensuring continuity of measurements. During this period, the difference (bias) between Jason-2 and Jason-3 for Ku-band backscatter (Sig0) was within 1 dB. The difference in the brightness temperature measurements was within 3 °K.

For this study, the satellite radar measurements were extracted from the geophysical research data records product (GDR) distributed by AVISO+ data portal (avisoftp.cnes.fr, last access 2020/03/20). The GDR product contains various parameters estimated from the radar return echo, which is represented as a waveform. In our study, we used the 20 Hz backscatter coefficient retrieved by the ICE1 algorithm. The AMR measurements of the brightness temperature have a 1 Hz temporal frequency. They were linearly interpolated to the coordinates of the 20 Hz radar measurements.

High-resolution optical Landsat 8 images (https://earthexplorer.usgs.gov/) were used for the geographical selection of altimetric radar and radiometer measurements over river channels using our own Python code that overlaps along-track Jason measurements and Landsat images. The cross-section of an altimetric track with a river channel is called a virtual station (VS). The VS received a name containing the track number. To distinguish the VSs located on secondary branches from those located on the main Ob River channel, the station names were extended with the corresponding index "S_Ob" (if necessary).

3 Temporal variability of radar altimetry signal over frozen rivers

3.1 Backscatter variability

In our previous studies (Kouraev et al., 2005; Zakharova et al., 2019, 2020), we noted that over Arctic rivers, the returned altimetric radar signal (expressed as backscatter) has specific seasonal behaviour. This behaviour is strongly related to the hydrological phases, especially the presence of ice. In contrast to side-looking SAR instruments, for nadir-looking altimetric radars, smooth surfaces produce a higher return echo than rough surfaces. High backscatter values of nadir-looking altimeters were observed when the instrument footprint contained a large fraction of calm water. Over large flooded areas, the water surface exhibits a certain roughness owing to turbulent flow and wind and, thus, produces low backscatter values. The presence of floating ice, frazil, or slush prevents the development of wind waves and increases the specularity of water. The installation of ice cover in river channels starts from the banks (where the turbulence and flow are small) by the formation of a fine skim ice with a smooth surface and bottom. This ice grows in area and thickness, intercepts, and accumulates floating frazil flocks and ice floes (Hicks, 2009). During periods of snow accumulation, shuga (new ice, composed of spongy, white lumps a few centimetres across resembling slushy snowballs) forms and drifts along the river. Drifting ice contributes to the growth of border ice, reducing the open water area and leading to the formation of ice dams (bridging). The bridging starts at tight bends or at narrow channel locations. Both water with drifting ice and skim ice provide strong return altimeter signals. At this time of their appearance in late autumn, the peak on the backscatter time series indicates the start of freezing (Figure 3).

River ice mainly grows as water at the bottom of the ice cover (called congelation ice) freezes, and the latent heat of crystallisation is conducted upwards through the ice and snow to the atmosphere. Growth can also occur on top of the ice cover when the snow load or hydrostatic pressure is high, and water seeps through cracks, wetting the snow. The wet snow refreezes forming porous white ice, which is called snow ice. As ice grows and the volume scattering

of the radar echo within ice increases, the backscatter decreases and forms a well-detectable winter recession limb on the backscatter time series (see the red lines in Figure 3). On the Ob River, the ice gains approximately 30% of its total thickness during the first freezing month. The highest temporal changes in backscatter ($\Delta Sig0/\Delta t$) are observed during that period. The $\Delta Sig0/\Delta t$ value reduces if the open water (polynya) persists because of the high local velocities or tributary inflow. As the real orbits of the Jason satellites have a 400 m cross-track oscillation, the fraction of open water of polynya within the footprint can vary from cycle to cycle, resulting in secondary peaks on the backscatter winter recession lines. Small winter peaks can also appear due to the redistribution of snow on the ice surface, snow wetting during mechanical ice cracking in winter, and occasional snow melt during warm sunny days in spring (see Figure 3b).

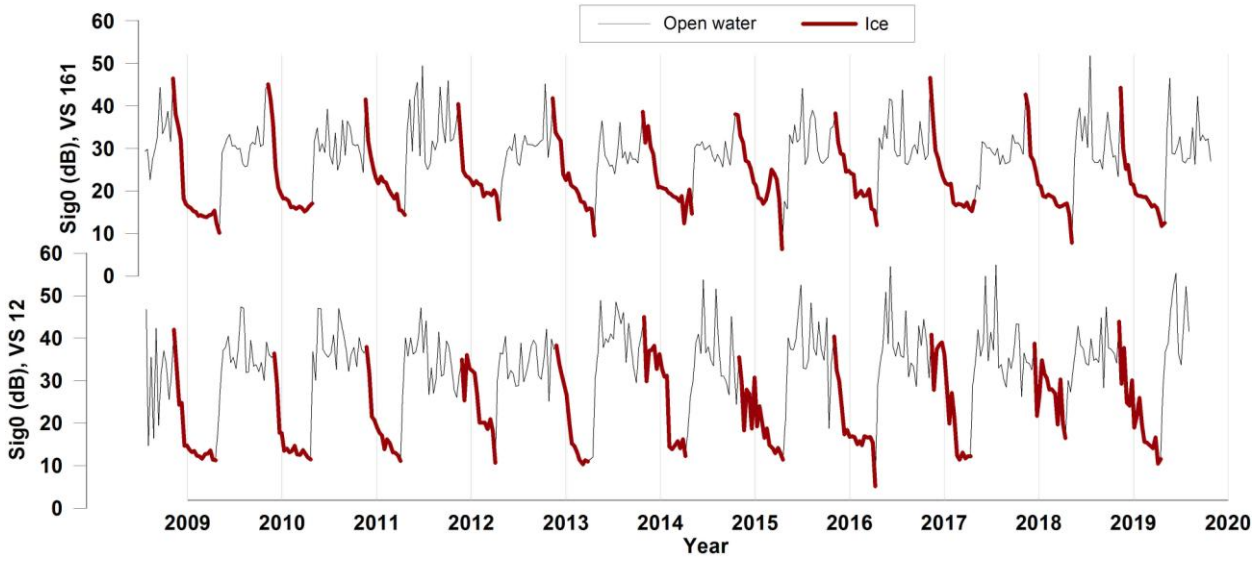

Figure 3: Variability of backscatter at VS 161 (a) and VS 12 (b) (see Figure 1 for VS locations). Data for period of ice cover are shown as thick dark red line.

River ice break-up is influenced by both thermodynamic and hydrodynamic processes, known as thermal and mechanical break-up, respectively. First, when air temperatures are still mostly negative, ice undergoes metamorphism under the influence of solar radiation. At that time, a drop in backscatter in the order of 5-10 dB can be observed (see, for example, 2012-2016 years in Figure 3a). Similar phenomena have previously been observed on Lake Baikal ice using SARAL/AltiKa altimeter data (Kouraev et al., 2015). When air temperatures become positive, snow on the ice surface melts, increasing the surface backscattering of the radar signal. Melting progressively affects the ice, and vast melt ponds can appear on the ice surface, leading to an increase in the backscatter coefficient.

Mechanical breakup starts when the water level rises. Water can flood the ice surface due to previous flooding on tributaries or due to leakage through cracks in weakened/fractured ice. A high (>25 dB) backscatter peak occurs at the beginning of the flood. The value of the peak ranges from to 25-50 dB, depending on the stage of breakup and river morphology (channel width, banks, oxbow lakes). As the water becomes free of ice, the backscatter decreases owing to the increased surface roughness induced by wind and turbulence. During the open water season in summer, several peaks are frequently observed. The summer variability in backscatter depends on many factors, including, but not limited to, VS location (banks, presence of islands, floodplain characteristics), the proportion of water within the footprint (intermittent summer rain flood inundation), and wind influence.

3.2 Waveform changes

The radar altimetry return signal is represented as a waveform (return power variation across time) (Figure 4). The shape of the waveform varies for different types of surfaces and can provide a variety of information useful for the interpretation of geophysical processes. When estimating lake ice thickness, Beckers et al. (2017) found the presence of an intermediate peak on the leading edge of the waveform. The authors interpreted this peak as backscattering from the air/ice or air/snow interface (ice surface), while the main peak is considered to originate from the ice/water interface (ice bottom). On many of the radar waveforms we extracted over river ice, we also detected this intermediate peak on the waveform leading edge (Figure 4). Considering that the radar echoes over rivers come from very heterogeneous surfaces, we avoid referring this peak to any definitive reflecting boundary and suggest another approach. Figure 4 demonstrates that during ice growth, the main waveform evolution is related to a decrease in power of waveform main peak. This can be explained by the signal volumetric scattering within the growing ice. We noted that the decrease is proportional to the value of the backscatter (which can be seen as the integral under the waveform). Based on this observation, we propose to retrieve the ice thickness by establishing a simple statistical relation between radar backscatter and river ice thickness.

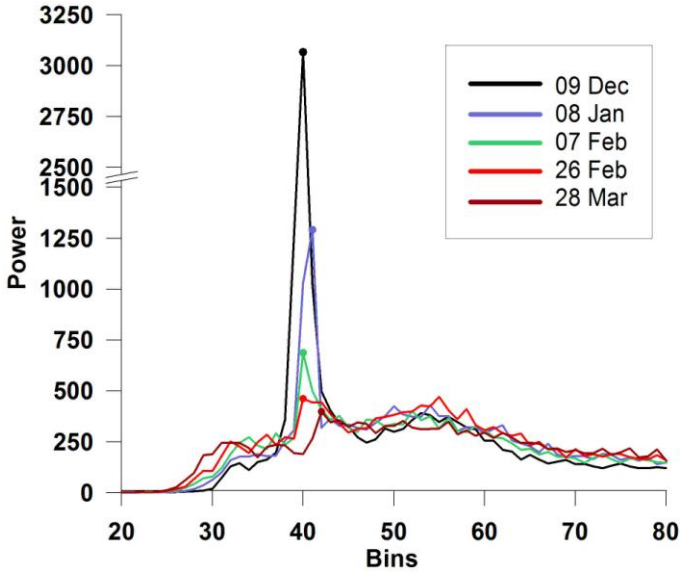

Figure 4: Winter evolution of typical waveforms for track 88 (see Figure 1) over a river channel. The coloured lines correspond to different dates of the winter 2013-2014.

4 Methods

4.1. Ice onset and break-up algorithm

Considering the behaviour of the backscatter over frozen rivers described in Section 3.1, we developed a dynamic algorithm for retrieving ice phenology dates based on the analysis of Sig0 time series specific for each VS. We suggested that the last annual peak of each year in the backscatter time series corresponded to the beginning of river ice formation. In the case of a multi-peaky recession limb, see for example VS12 in 2013 (Figure 3b), we selected the peak height of the order of spring-summer peak heights typical for this VS. If the selection of the peak was not straightforward (for example, two high peaks within one month or the prominence of the peak was low), an additional criterion based on the brightness temperature difference between the 34.0 and 18.7 GHz frequencies (ΔTB) was introduced. We select the backscatter peak at a time t, if in a time frame of (t-1, t+2) satellite cycles at least three of the four ΔTB values are <2° K. Radiometric brightness temperature measurements integrate emissions

from larger surrounding areas than altimetric radar backscatter measurements. Freezing on the floodplain and banks usually occurs earlier than in the river channel. By applying the (t-1, t+2) window, we ensured that the freezing in the area of the VS progressed, and the backscatter peak was not caused by a synoptic-scale cooling episode or by calm weather conditions.

The beginning of the ice cover decay (thermal melting) marks the beginning of the spring backscatter increase. The melt-detection algorithm searched for the spring peak in the backscatter time series. For multi-peak winters, the algorithm also uses the ΔTB condition. In this case, the algorithm searched for the peak which is accompanied by a simultaneous increase in ΔTB in the order of mean summer ΔTB for a given VS. In a few instances, the spring peak was absent or could not be automatically detected because of a low prominence. In these cases, we used the date of maximal increase in backscatter between two satellite cycles ($\Delta Sig0/\Delta t$) for the period from January to mid-June.

A variety of combinations of different geomorphological (banks, floodplain, river width, islands), meteorological (synoptic cooling/warming episodes), and ice cover (polynya, ridging) conditions can exist. Their complex impact on the backscatter variability during freezing and melting makes it difficult to address all variations in an automated manner. Because of this, we decided to compare the performance of the proposed automatic freeze/melt detection algorithm with its manual implementation: visual analysis of time series and detection of melt/freeze dates based on the described criteria.

4.2 Ice thickness algorithm

Year-to-year variations in the backscatter values at the beginning of the freeze-up period (Figure 3 a, b) may be caused by different land/water/ice proportions within the radar altimeter footprint, wind conditions, floating ice concentration, etc. Assuming that the decrease in backscatter between two consecutive observations ($\Delta Sig0/\Delta t$) is proportional to the gain in ice thickness (see Section 3.2), we used a relative backscatter decrease instead of the absolute backscatter values. This allowed us to reduce the effect of the initial freezing conditions on the accuracy of retrievals. Starting from the first date of freezing, we estimated the backscatter cumulative difference $\Sigma(\Delta Sig0/\Delta t)$ and constructed the relationship between this parameter and in-situ ice thickness (Hice) measured at the nearest gauging station. The application of a locally estimated scatterplot smoothing (LOESS) filter on the $\Sigma(\Delta Sig0/\Delta t)$ parameter made it possible to minimise the effect of secondary peaks on the backscatter winter curve (see Section 3.1).

Along the 400 km long Low Ob River reach covered by the 20 northernmost Jason satellite tracks, 48 VSs were defined using overlapped Landsat 8 images and Jason-2 and 3 tracks (see Figure 1). The ten VSs nearest to the five gauging stations were chosen as a training set for the calibration of the ice phenology dates and ice thickness retrieval algorithms and for the estimation of uncertainties. The results of the retrievals of ice onset and ice melt dates by both the automated and manual approaches were compared to the ground station records of ice types or water/ice cover state (ridging, polynya, water-on-ice, ice drift, etc.). As the dates of in-situ measurements do not coincide exactly with the Jason overflight dates, ice thickness values were linearly interpolated between two adjacent dates of in-situ observations for the dates of satellite overpasses. The other 38 VSs (main set) were used to characterise the ice conditions within the entire studied river reach.

Power equation (1) produced the best fit between the cumulative backscatter difference and in-situ ice thickness measurements.

$$Hice\_alti = a \times abs(\Sigma(\Delta Sig0/\Delta t))^b \quad (1)$$

The coefficients a and b of the equation were estimated for each pair of gauging VSs from the training set. Using the leave-one-year-out method for each (Picard and Cook, 1984) VS - gauge station pair, we obtained a set of a and b coefficients and estimated their mean values. These average values were then used for ice thickness estimation on the corresponding training VS. The accuracy of the ice thickness retrievals were evaluated using the correlation coefficient and root mean square error (RMSE) calculated between retrieved and observed ice for the 2008-2018 period.

Obtained coefficients a and b were applied to other 38 VSs of the main VS set. To do this, we constructed a Sig0 correlation matrix for all VS. Then, for each VS from the main set (VS_i), we used the coefficients a and b of the VS from the training set (VS_{jt}), which expressed the best correlation between $Sig0_i$ and $Sig0_{jt}$. Finally, we used the estimated ice thickness at all 48 VSs to develop weekly ice maps covering the 400 km Low Ob River reach. A schematic representation of the processing steps is presented in Figure 5.

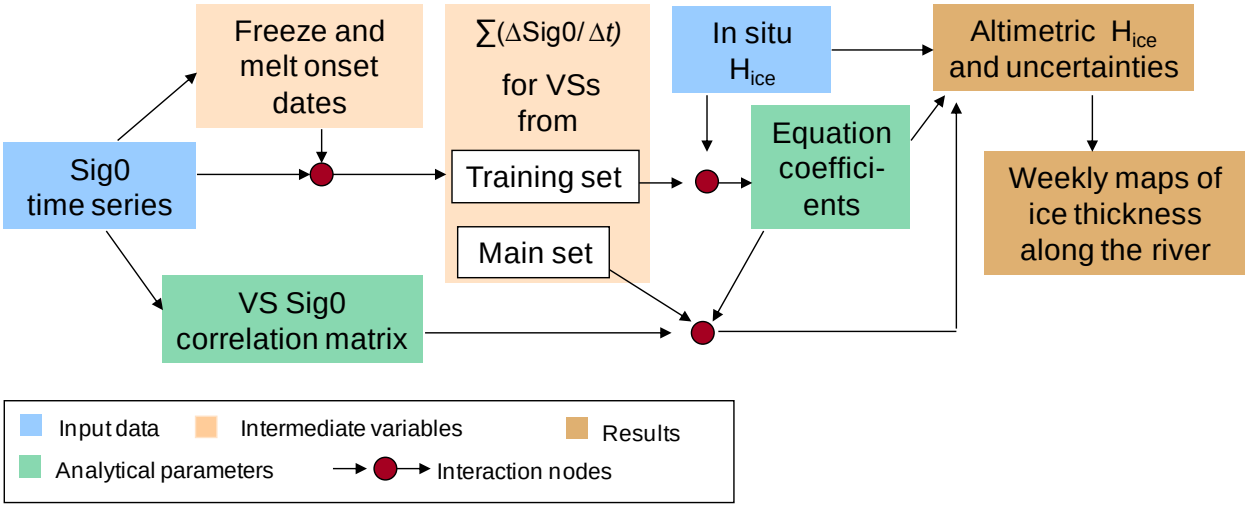

Figure 5: Processing scheme of ice thickness retrievals from altimetric radar measurements.

5 Results

5.1 Ice phenology algorithm verification

The ice onset was well detected by the Jason radar altimeter. Considering the 10-day repeat overpass of the satellite and the distance between the gauging stations and VS, we considered a 10-day time-step difference (e.g. ±10 days) as an acceptable accuracy for altimetry-derived ice phenology dates. For 90% of the retrievals using the visual backscatter time series interpretation (manual routine), the difference in the first ice events with in-situ observations was less than 10 days (Figure 6a). In 56% of the cases, the difference was 0 days. As the radar footprint over rivers is heterogeneous and is affected by signals from the frozen/unfrozen state of land/river/floodplain lakes, there are numerous variations in the behaviour of backscatter at the beginning of the freeze-up period. At this time, the automated routine misses certain behaviour types, and detection is less accurate for the first ice appearance than in the case of the manual routine. Only 70% of the altimetric freeze-up dates fell within 10 days of the in-situ observations at gauges, and only 40% fell on the same day.

Break-up is a more complex process consisting of the thermal degradation of ice cover (melt start) and its mechanical break-up and downstream movement (melt end). Comparing the dates of altimetry-derived melt onset with the ice state flags provided by gauging stations, we can conclude that the manual routine of our algorithm accurately detects the start of ice thermal degradation. In 88% of the cases, the difference between the manually

retrieved melt dates and in-situ observations of the first water appearance was less than ±10 days (Figure 6b). The automatically derived melt date estimations were less accurate for the detection of melt starts compared to the manually derived estimations. However, the automated approach was more adapted for the detection of the melt end than for detection of melt start; an acceptable accuracy of less than ±10 days was achieved for 67% of cases (Figure 6 b, c). Manual estimation of dates associated with freeze-up/break-up allows for better control of the complex behaviour in backscatter and, consequently, the handling of unrealistic retrievals than automated estimation. The automatic approach can pass over complex cases and detect unrealistic early/late dates. For the 48 VSs on both the main and secondary channels, over the full 10-winter period of study , the automated algorithm failed, that is, detected unrealistic melting/freezing dates, before 10 April and after 10 June, respectively, in 10% of cases.

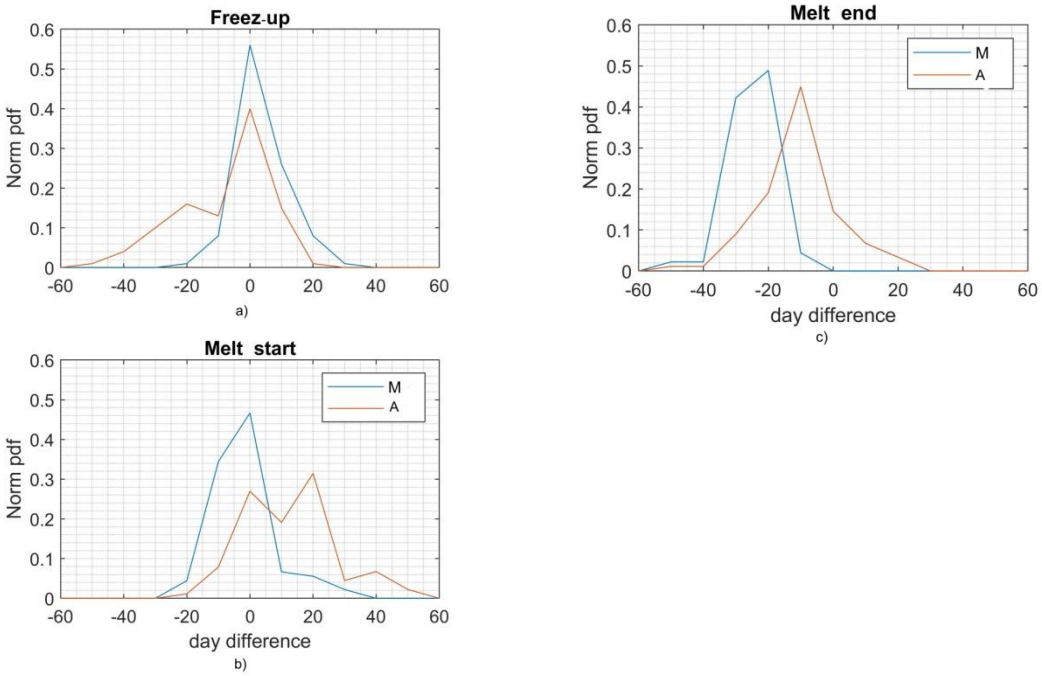

Figure 6: Normalized distribution of difference between altimetric and *in situ* observed dates of freeze-up (a), melt start (b) and melt end (c) for 2008-2019 for 10 virtual stations from training set of VSs. M - manual routine, A - automated routine.

A comparison of the interannual variability of median dates estimated for VS located on the main river branch (20 VS in total) with the corresponding parameter estimated from observations at four gauging stations (also located on the main river branch) demonstrated good agreement between satellite retrievals and in-situ observations (Figure 7). A significant difference between gauging and VSs (on the order of 20 days) was observed only for melt start dates in 2014. This good agreement suggests that our algorithm is capable of monitoring the interannual variability of ice events.

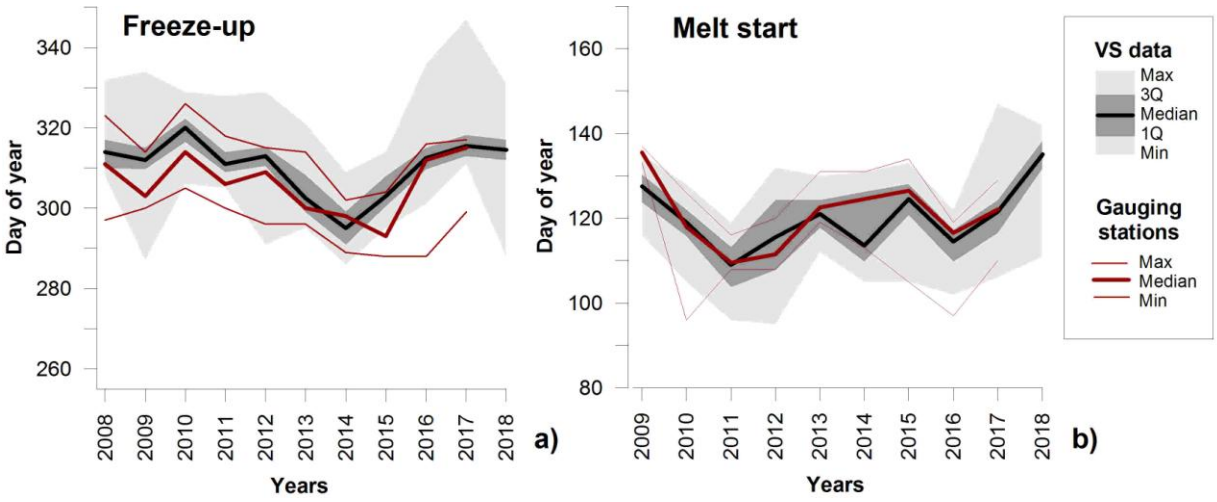

Figure 7. Interannual variability of altimetry-derived dates of freeze-up (a) and melt start (b) from manual approaches for the main Ob River channel. Red lines are the median (bold line) and the min-max values (thin lines) observed on four gauging stations along the main Ob River channel. The black line corresponds to the median value of dates observed at 20 virtual stations within the same river reach. The dark grey zone is the spread between 3rd and 1st quartile, and light grey zone is the spread between minimum and maximum values.

5.2 Ice thickness retrievals

The accuracy of the ice thickness retrievals from altimetric measurements was estimated for the ten VSs from the training set located around the gauging stations. At the northern VSs (VSs 161, 138, 237S_Ob, and 249S_Ob), the correlation between retrieved and observed ice thickness was stronger than at other locations, and the errors in estimates of the altimeter-retrieved ice thickness were less than 0.12 m (Table 2). For the southernmost VSs (VS 12 and 109), the error increased up to 0.14-0.18. For many years and many locations the uncertainty in ice thickness estimates is higher at the beginning (low Hice) and at the end (high Hice) of the ice period, compared to the Hice retrievals in the middle of winter (Figure 8). Inaccurate detection of ice onset can affect the accuracy of thickness estimates, especially at the beginning of the freeze-up. Another reason for the increased errors is the multi-peak character of the backscatter winter recession curve and the residual noise present in the backscatter time series after the application of the smoothing procedure. This occurs, for example, at VS12, where a polynya persisted until March in at least four years of the study period, producing a noisy backscatter time series in winter (see Figure 3b) and a high dispersion of points around 1:1 line on the Halti - Hinsitu scatterplot (Figure 8).

Except for VS109, the variability in the values of coefficients a and b in Equation (1) is low (Table 2), which indicates good stability in the established relationships and their potential validity for other VSs located far from the gauged reaches. One way of verifying the sensitivity of the Hice_alti retrievals to fitting parameters consists of applying the coefficients obtained for an adjacent VS located in the north (or south, respectively) from a VS under consideration (see cross-validation columns in Table 2). Similar scores obtained in cross-validation experiment demonstrate a robust equation (1) fitting and resulted low errors in Hice_alti estimation for the northern VSs (161, 138, 237S_Ob, and 249S_Ob). The results for the southernmost VSs are not as good. However, the retrievals at the southern VS in the cross-validation experiment could be improved by selecting the equation parameters (a and b) not from the closest VS, but from the training VS which expressed the best Sig0 correlation with the Sig0 of VS considered. For example, when applying the equation built for VS135 - Gorki gauging station pair to VS109 and

VS12 (backscatter of the VS135 demonstrated the highest correlation with the backscatter of the VS109 and VS12), the RMSE of retrieved Hice_alti for these VSs decreases from 0.23 to 0.18-0.19 m (see scores in the denominator of corresponding lines in Table 2).

Table 2. Coefficients a and b for built relations, correlation coefficient (R) and RMSE between retrieved and *in situ* ice thickness for virtual stations from training set (left panel) and for cross-validation experiment (right panel). S_Ob refers to VS stations located on the secondary river branch (see fig.1)

Virtual stations	Corresponding gauging station	a	b	R	RMSE, (m)		VS for cross-validation equation	R cross-validation	RMSE (m) cross-validation
161	Pitlar	8.69	0.39	0.94	0.07		138	0.94	0.09
138	Pitlar	6.54	0.42	0.94	0.07		161	0.94	0.09
237 S_Ob	Muzhi	7.64	0.42	0.90	0.10		240 S_Ob	0.90	0.10
240 S_Ob	Muzhi	7.96	0.41	0.90	0.10		237 S_Ob	0.89	0.11
240	Gorki	7.70	0.39	0.81	0.12		135	0.81	0.13
135	Gorki	6.88	0.42	0.87	0.11		240	0.87	0.11
164	Kazym Mys	8.83	0.35	0.84	0.10		211	0.84	0.10
211	Kazym Mys	10.7	0.31	0.76	0.12		164	0.76	0.13
12	Polnovat	8.23	0.41	0.77	0.18		109/135*	0.76/0.76*	0.23/0.18*
109	Polnovat	2.92	0.55	0.84	0.14		12/135*	0.76/0.76*	0.23/0.19*

* two equations built for corresponding virtual stations are used for cross-validation.

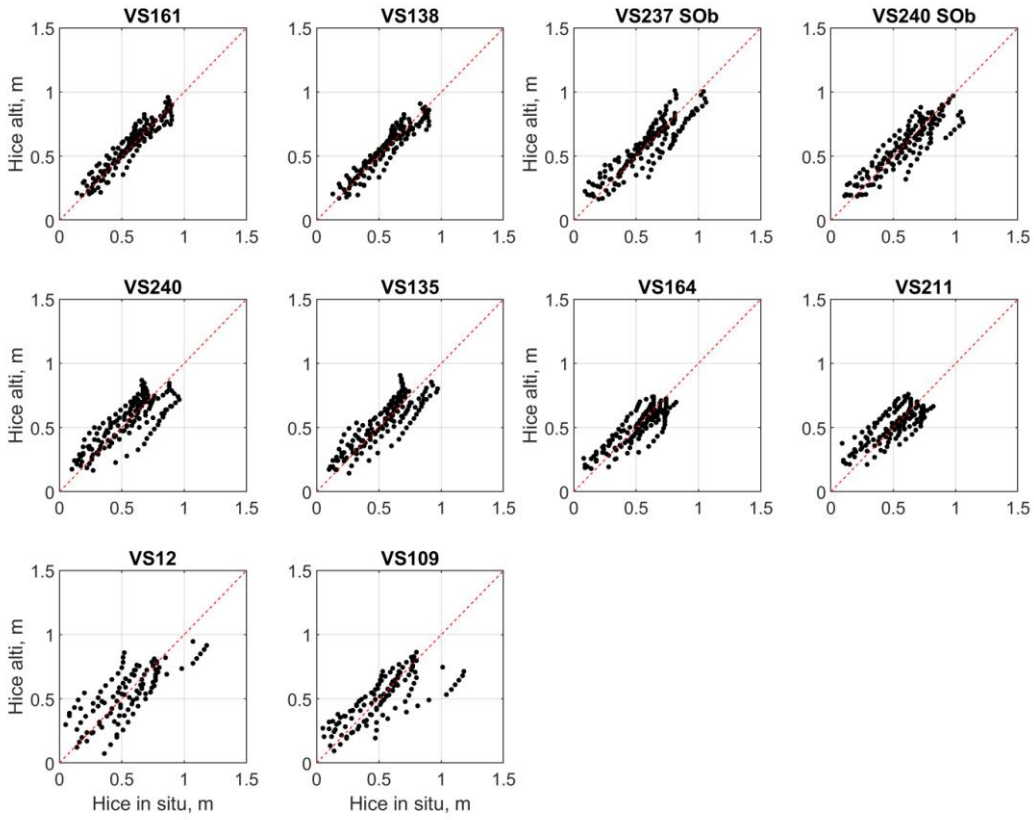

Figure 8. Ice thickness observed at gauging stations and retrieved from the backscatter measurements for training VSs. The red dash line is the 1:1 relation line.

5.3 Ice thickness estimation for the entire studied river reach

Using the coefficients a and b of Equation (1) developed for the VS from the training set, we estimated the ice thickness at locations of the other 38 VSs. Based on the results of the cross-validation test, the following strategy was adopted: firstly, for each VS, using the correlation matrix, we searched for the best correlation between its backscatter and the backscatter at one of the training VS(VS_t); then, the coefficients a and b of VS_t showing the highest correlation coefficient were applied to the VS considered.

Ice thickness retrievals at all 48 VSs were then used for the creation of weekly maps, which were generalised into a 2D spatio-temporal ice thickness product (Figure 9). For this, the altimeter-derived ice thicknesses were interpolated and smoothed in 2D spatio-temporal coordinates using a moving average filter with a window size of 40 km/30 days. The size of the applied window allowed for a) preserving as much as possible the magnitudes and the spatial heterogeneity of ice thickness in the spatial domain, and b) to reduce the residual noise in the temporal domain left after smoothing of the backscatter time series with the LOESS filter.

The along-river variability in ice thickness, controlled by local morphological factors, can be important. In the absence of validation data for the retrieved ice thickness for inter-station areas, we suggest examining the interannual dynamics of two parameters derived from altimetric and in-situ observations: the maximum ice thickness and ice thickness observed on 1 December. From a practical standpoint, knowledge of the maximum river ice thickness is relevant for hydro-climate change monitoring, while the ice thickness determined on 1 December is

crucial for local and regional socioeconomic stakeholders, as this is the average date for the opening of the ice bridge road to the north of the study area at Salekhard.

The interannual variability in maximum ice thickness retrieved from altimetric measurements at more than 90% of the VSs indicates a clear decrease from 2008 to 2012 (Figure 9). This tendency corresponds well to those observed at all gauging stations in the study region (Figure 10a). Since 2013, the maximum ice thickness has increased slowly. However, altimetric and in-situ observations after 2013 both exhibit spatiotemporal variability that is not always in agreement. This disagreement may be related to environmental factors affecting ice growth such as snow amount, autumn ice drift and accumulation, ridging/hummocking, and ice flooding (water-on-ice). For example, according to station records, ridging events appear more frequently after 2012 at the northernmost gauging station, Pitlar, than at other gauging stations. We cannot fully exclude the effect of the simplicity of the retrieving algorithm based on the empirical approach as well as the effect of spatiotemporal smoothing of the altimetric retrievals used in map production.

The difference between altimetric and in-situ ice thickness at 1 December observed in their interannual variability lies within algorithm uncertainties 0.07-0.18 m (Figure 10b). In addition to the geophysical reasons and algorithm simplicity noted above, the observed difference can be related to the degradation in the quality of the in-situ time series (gaps, unrealistic values) and the low representativeness of the one-hole sampling protocol.

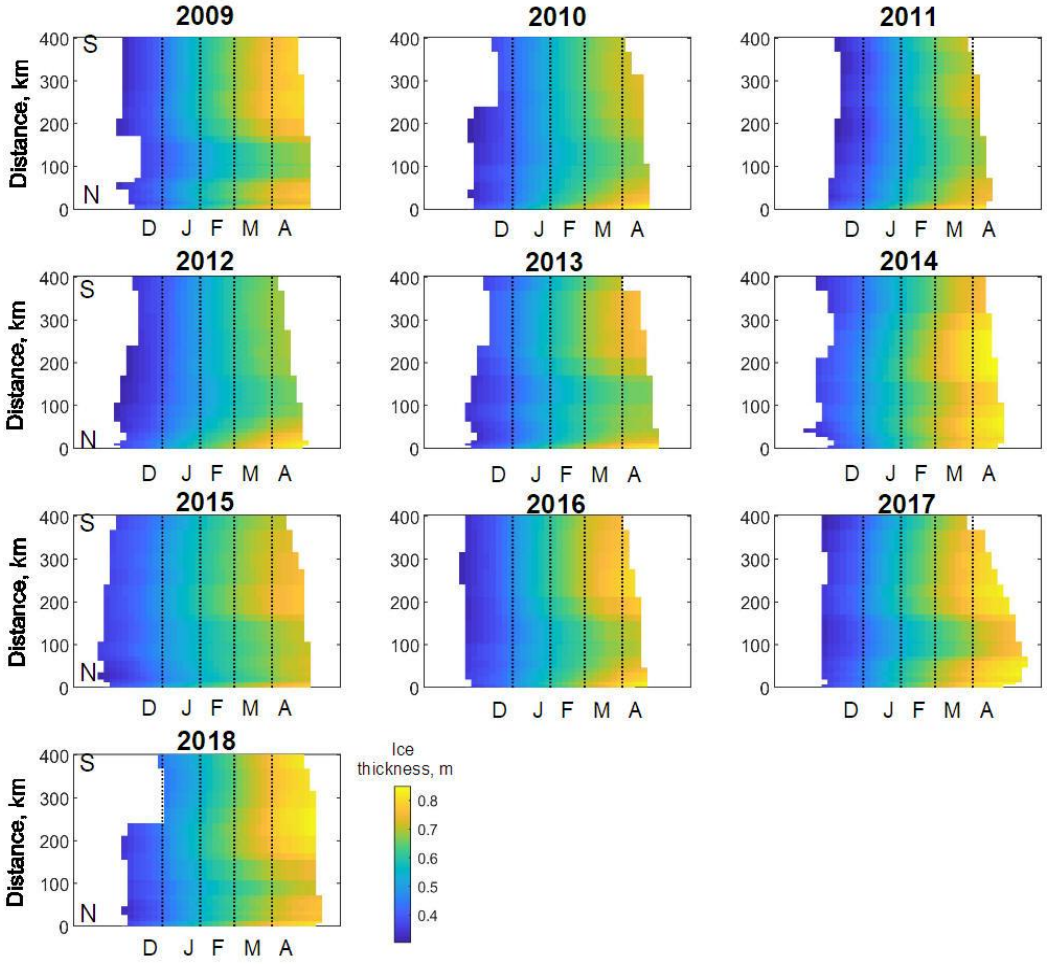

Figure 9. Spatio-temporal ice thickness variability (m) for the main branch of entire Low Ob River reach for the 2008-2018 period from generalized weekly altimetric product. Distance in km is indicated from the northernmost virtual station 187 in the direction upstream (south). Letters on X-axis – first letter of month (January-May).

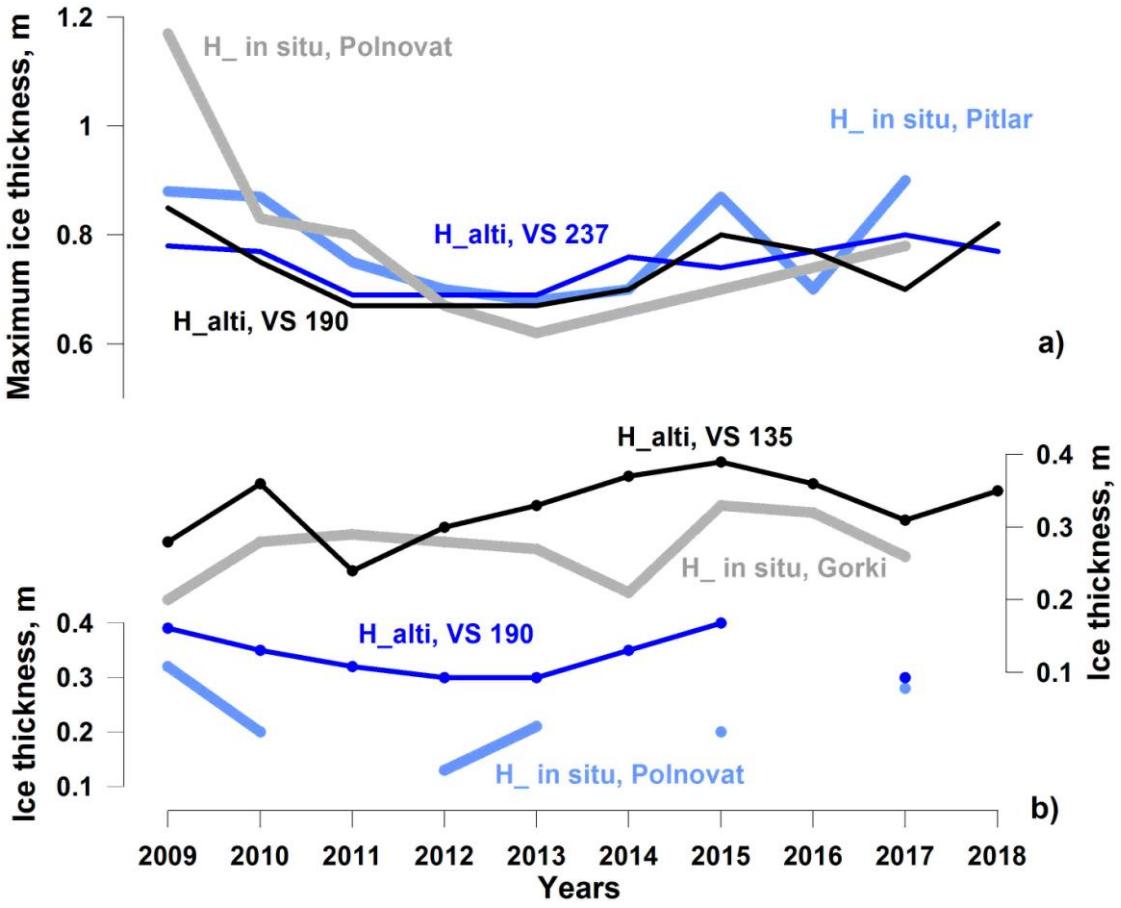

Figure 10. Interannual variability of ice thickness extracted from altimetric 2D ice thickness product at VS 237, 190 and 135, and observed at gauging stations: a) maximum ice thickness, b) ice thickness at 1 December.

5.4 Winter ice bridge roads operation forecast

In many regions with seasonal ice cover, frozen rivers enhance the interconnection and supply of many small, and even some large, cities. Many remote villages that in summer are linked to supply centres only via expensive helicopters or boat transport, have the opportunity to directly access the main land transport arteries using frozen-ground and ice roads. The importance of ice roads is highest for the Arctic regions, where the construction of permanent bridges is restrained by the presence of permafrost and its destabilisation.

A good example is the Salekhard City located in the north of the Ob River near the polar circle in the zone of discontinuous permafrost. The city has 50 000 inhabitants and is supplied primarily via the Northern Railway, which connects the small town Labytnangi on the left bank of the Ob River with the European part of Russia and the main supply centres. Merchandises from Labytnangi are delivered to Salekhard by ferry. Every winter, an ice road is constructed to ensure the transport of goods and people. Owing to security reasons, the ferry ceases operation after

the appearance of the first ice. The ice road construction (artificial growing of ice thickness via pumping of water on the ice surface) begins when the ice thickness attains an allowed value of 0.20-0.25 m (Instructions on safety organisation, 1969). The traffic of light vehicles is allowed when the ice thickness exceeds 0.30 m. The ice road operation usually starts 3-4 weeks after the beginning of freezing, with an average of 30 November-1 December. The road operation closes gradually starting from the limitation of the lorry load in the middle of April until full halt at the beginning of May. The ferry connection is restored approximately three weeks later. Between the ferry and the ice road operation, the connection is ensured via a hovercraft boat only for a limited number of passengers or for emergencies.

The dates of the autumnal halt of ferry operation for 2010-2018 agree very well with dates of the first ice occurrence on four northernmost tracks of the Jason satellite located 65-75 km south of the city. For the short-term forecast, the satellite observations on VS 112 and 9 are especially good and can predict the end of ferry operation on average 4 days ahead. We assumed, further, that an average value of the dates when Hice_alti at the four northernmost VSs reached 0.30 m may provide an estimate for the road opening date. Using this criterion, we predicted the beginning of ice road traffic with an average accuracy of four days. However, in half of the years, the predictions differed from observations by more than five days (11 days maximum). As noted in Section 5.2, at the beginning of freezing, the errors of Hice retrievals are quite high, and ice thickness is often overestimated. Based on this fact, we consider that at the moment the altimetric algorithm and the ice thickness product are not sufficiently accurate for the ice road opening forecast. Nevertheless, their accuracy is sufficient for the assessment of climatic perspectives as we capture the interannual variation of dates of ice road opening (Figure 11a).

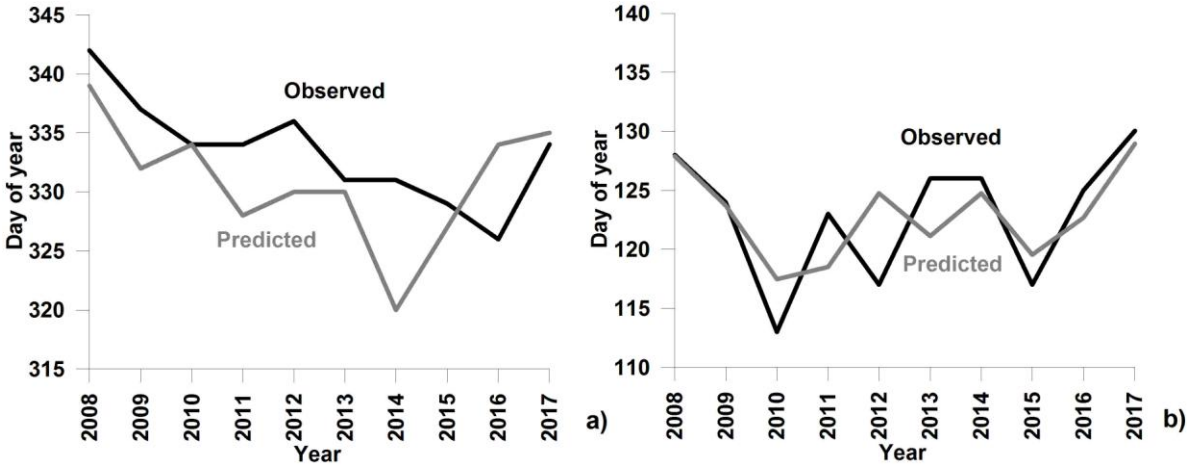

Figure 11. Observed and predicted dates of ice road opening (a) and closing (b).

For the prediction of dates, when the ice road at Salekhard ceases its operation, the use of the northernmost VSs is not possible as hauling on the ice road closes before the altimeter detects the melt onset in this reach. However, information on the melt onset at VSs located in the lower reaches can be applied. Using altimetric retrievals of the melt start for the entire set of 48 VSs, for each year, we searched the date when at least two altimetric melt onsets (AMO2) were detected within the entire 400 km river reach. This date serves as a predictor of the date of ice-road closure at Salekhard. The correlation between AMO2 and observations was significant (p-value = 0.025) at correlation coefficient 0.70 (Figure 12a). After applying a correction to AMO2 computed from the relationship in Figure 12a, we obtained forecast dates of ice road closing at Salekhard with an RMSE of 3 days (see Figure 11b). The leading time of the forecast can be determined from the plot shown in Figure 12b. It varies from 4 days (for late melting start) to 22 days (for yearly melting start).

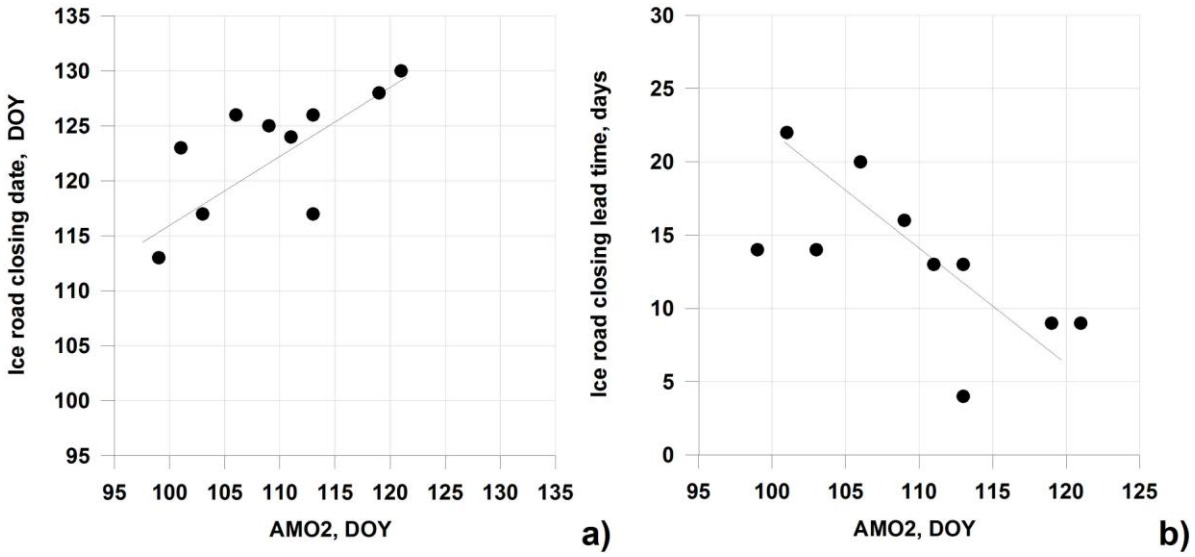

Figure 12. Relation between altimetric melt start onset dates (AMO2) and Salekhard ice road closure dates expressed in days of year (DOY).

6 Discussion

6.1 Factors affecting ice thickness retrievals from altimetry

Various factors can affect radar signal return echo and, consequently, the accuracy of river ice thickness retrieval. One source of uncertainty could originate from the underestimation of the role of snow-on-ice in microwave signal scattering (King et al., 2013, 2015). However, Willatt et al. (2011) demonstrated that the Ku-band electromagnetic wave scattering by snow at nadir is low, and in our study, we neglected the presence of snow on ice. Using precipitation data from the nearest meteorological station, we noted that not all heavy snow accumulation episodes affected the backscatter over river ice. In several cases, snowfall resulted in backscatter changes in the order of 1.5 dB. The smoothing procedure applied to the cumulative $\Delta Sig0/\Delta t$ series helped to eliminate this effect. Moreover, after adding the in-situ snow depth to the ice thickness, we noted that the Hice - $\Sigma(\Delta Sig0/\Delta t)$ power relationship becomes weaker.

Another factor potentially affecting the backscatter value over freshwater ice is ice roughness at the ice/water interface (Atwood et al., 2015). The roughness of the ice bottom on the rivers is expected to be high at the beginning of the freeze-up period in bridging areas, where floes juxtapose and accumulate underside. Any rough boundary dissipates the signal of nadir-looking radar instruments, resulting in a decrease in backscatter. Further congelation of the inter-floes volume as well as ice growth both lead to levelling of the ice low boundary. We suppose that the under-ice current may also contribute to the ice bottom levelling in the Ku-band radar wavelength scales (~1-1.5 cm). This levelling would increase the radar return power during winter. However, we did not find evidence of this process in the backscatter time series (see Figure 3). Either the levelling effect is weak and is masked by high volumetric scattering of the radar echo within thickening ice, or at the location of our VSs, the ice juxtaposing (and consequently the ice bottom roughness) is unimportant. Future investigations with dedicated in-situ observations on river ice texture evolution are needed to understand the effect of bottom roughness on radar altimeter return signals.

Ice internal layering is also important for the scattering of radar signals (Legrésy et al., 1997; Nilsson et al., 2015; Slater et al., 2019). Under the climatic conditions of northwestern Siberia, ice layering (characterised by dense

reflective icy surfaces) is rare, as the air temperature of winter warming episodes never approaches the melting point. Daily positive temperatures lasting several hours can occur starting from the end of March in the southern portion of the study area and 1-2 weeks later to the north. During this time of the year, the ice was well developed and almost reached its maximum thickness. Layering can also occur after river water floods the ice surface through cracks. According to in-situ observations at gauging stations, this phenomenon was observed in the last several years at the end of the ice season in the southern portion of the study area. Both warming episodes and flooding events lead to a backscatter increase in the order of 1-5 dB and render altimetric ice retrievals difficult by the end of the ice season. The highest underestimation of Hice (0.15-0.20 m) was observed in such cases.

The internal ice structure can also affect the backscatter value, for example, via air bubble inclusion (Gunn et al., 2018). During ice formation, jamming and ridging, can occur in Arctic rivers, resulting in the formation of air pockets. Ridging is rare in gauging stations on the Ob River. However, there is no information about the state of the ice at other ungauged reaches, including the areas covered by VSs. We can only speculate that ridging/hummocking could be one of the reasons for the high difference in the coefficients of Equation (1) determined for VS109. On Landsat-8 images acquired for two springs on 2019/04/25 April and 2015/05/01 (not shown), the irregular spatial ice structure in the area of VS109 indirectly confirms our hypothesis. More studies involving the simultaneous analysis of SAR imagery showing ice field irregularities (Unterschultz et al., 2009) and altimetric signals could help to clarify this issue.

6.2 Potential improvements of algorithms

The results obtained demonstrate that the altimetric retrievals of ice phenology dates and thickness are capable of representing the interannual variability of these parameters and can be potentially used in climate studies (see Figures 7 and 10a). However, for this first version of the product, we cannot recommend the use of ice thickness for winter road opening forecasts, as it seems that for many locations, we overestimate the thickness at the beginning of the freeze-up period (see Figure 10b). Several improvements are suggested for future studies. First, an improvement in the accuracy of detection of the freeze-up algorithm is envisaged. In our algorithm, the ice thickness estimation starts from the date of the first ice (bank ice or frazil floes) appearance. Usually, the river reach in the area of the VS at this moment is not fully frozen. The detection of the date of the first consolidated ice (e.g. fully frozen reach) may help to reduce the errors in the retrievals in a low range of ice thickness.

Another improvement consists of the use of other parameters of the altimetric radar waveform instead of (or in complement to) the backscatter coefficient. As shown in Figure 4, the main peak of the radar waveform decreases as the ice grows. We suppose that the amplitude of the main peak or the area under this peak may produce stronger relationships with in-situ ice observations than the backscatter coefficient. As shown in Figure 4, during winter, the main peak is the most variable part of the waveform. This peak corresponds to the return signals from the ice surface and the ice bottom at the nadir (Backers et al., 2016). The other part of the waveform collects the return signal from the surrounding (off-nadir) areas and also contributes to the total value of the backscatter coefficient. Any temporal changes in the state of surrounding areas that are different from the state in the near-nadir area (e.g. ice flooding or off-nadir polynya) lead to backscatter changes not related to ice growth. Consequently, the use of waveform parameters related to the main peak could reduce the errors in the Hice estimates. Unfortunately, these parameters are not directly provided in the AVISO+ Jason GDR product, but they could potentially be estimated from the initial waveforms.

7 Conclusion

The decreasing number of in-situ observations and degradation of the quality of their time series is a good argument for boosting the development of satellite methods for freshwater ice monitoring. The present study demonstrates the potential of satellite radar altimetry for monitoring river ice parameters such as freeze-up, break-up, and ice thickness for the large Arctic Ob River.

An algorithm based on the analysis of backscatter coefficients from the Jason-2 and -3 satellite altimeters provides an estimation of river ice onset with an accuracy of ±10 days (corresponding to the 10-day satellite overpass frequency) in 90% of the cases.

River ice melt consists of two phases: thermal degradation and mechanical break-up. The algorithm detects the beginning of thermal degradation well with the same accepted accuracy of ±10 days for 88% of the cases. River ice thickness was retrieved from altimetric backscatter measurements via simple empirical relations with in-situ observations. The accuracy of the thickness retrievals (expressed as RMSE) ranges from 0.07 to 0.18 m.

The spatiotemporal smoothing of satellite-derived river ice thickness retrieved for 48 VSs along the 400 km reach of the Lower Ob River allowed for the elaboration of the weekly maps generalised in the form of an annual spatiotemporal product. The ice thickness time series could be extracted for any location and used for climate and ice road operational purposes.

Using this first version of the product, we demonstrated that the dates of opening of ice road near Salekhard City can be predicted from altimetric ice onset retrievals with an accuracy of 4 days. Errors in the prediction of dates of ice road closure were within 3 days. Despite these promising results, we consider that the current first version of the product is not sufficiently mature for operational use as it overestimates ice thickness at the beginning of the ice season. The accurate estimation of ice thickness is critical for safety. However, the algorithm and product could be significantly improved in the future through a multi-mission and multi-instrument (optical and/or SAR imager) approach. We are hopeful that with the use of the Copernicus satellite altimeters Sentinel-3A and 3B, an improvement in the retrieval of ice thickness can be made. These satellite missions carry more advanced altimetric SAR instruments with footprints representing a narrow band and return signals that are less contaminated by land than signals from the conventional Jason instrument. Although the nominal repeat frequency of the Sentinel-3 satellites (27 days) is not suitable for operational applications, they provide five overpasses within a 25 km distance around the Salekhard city ice road and, thus, the temporal resolution of observations may be significantly improved. The combination of data from the Jason and Sentinel-3 missions could be fruitful.

The Salekhard ice road is very well instrumented, monitored, and maintained by local authorities, thanks to the high demand for its use and high merchandise flow. In other regions, ice roads connecting small cities and villages are less monitored, and access to operational information is poor. Moreover, many intermittent and unofficial river crossings are developed each year by local people. Often, the lack of information on the state of ice results in accidents and requires intervention by the emergency service. The demonstrated capacity of the first version of the altimetric river ice product as a supporting tool for the ice road operation to the north of the Ob River is quite promising. Further product improvements and the development of sophisticated prediction criteria for road operation that could be adapted to other reaches of the Ob River are planned.

Acknowledgements. The authors express their gratitude to the staff of the State Traffic Service of Yamalo-Nenetzky Autonomous District (Russia) for providing the valuable information about ice road operation. The authors would like to thank the two anonymous referees for their helpful comments on our paper.

Funding. This research was made possible with support from RFBR project № 18-05-60021-Arctic, ESA (EO Science for Society Element) LIAM project (Contract No. 4000130930/20/I-DT) and ESA CCI Lakes+ (Contract No. 4000125030/18/I-NB –CCI+ PHASE1 – NEW ECVS - Lakes); the approbation of results was carried out in the framework of Governmental Program of Water Problems Institute, Russian Academy of Sciences, no № 0147-2019-0004.

Author contribution. All authors contributed to the data collection, algorithm development, analysis and presentation of results equally.

Declaration of Interests. The authors declare no competing interests.

References

Agafonova S.A. and A.N.Vasilenko, Hazardous ice phenomena in rivers of the Russian arctic zone under current climate conditions and the safety of water use. Geography, Environment, Sustainability, 13(2): 43–51, 2020.

Atwood D. K., G. E. Gunn, C. Roussi, J. Wu, C. R. Duguay, and K. Sarabandi, Microwave backscatter from Arctic lake ice and polarimetric implications, IEEE Trans. Geosci. Remote Sens., 53, 11, 5972–5982, doi:10.1109/TGRS.2015.2429917, 2015.

Beaton, A., Whaley, R., Corston, K. & Kenny, F. Identifying historic river ice breakup timing using MODIS and Google Earth Engine in support of operational flood monitoring in Northern Ontario. Remote Sensing of Environment, 224, 352–364, doi.org/10.1016/j.rse.2019.02.011, 2019.

Beckers J. F., J.A. Casey and C. Haas, Retrievals of lake ice thickness from Great Slave Lake and Great Bear Lake using CryoSat-2. IEEE Transactions on Geoscience and Remote Sensing, 55, 7, 3708-3720, doi: 10.1109/TGRS.2017.2677583, 2017.

Beltaos S., Hydrodynamic characteristics and effects of river waves caused by ice jam releases, Cold Regions Science and Technology 85, 42–55, dx.doi.org/10.1016/j.coldregions.2012.08.003, 2013.

Beltaos S., Carter T. , Rowsell R. , DePalmac S. G.S., Erosion potential of dynamic ice breakup in Lower Athabasca River. Part I: Field measurements and initial quantification. Cold Regions Science and Technology, 149, 16-28, doi.org/10.1016/j.coldregions.2018.01.013, 2018.

Chaouch, N., Temimi, M., Romanov, P., Cabrera, R.,McKillop, G., Khanbilvardi, R. An automated algorithm for river ice monitoring over the Susquehanna River using the MODIS data. Hydrological Processes, 28, 62–73, doi.org/10.1002/hyp.9548, 2014.

Chu T. Lindenschmidt K.-E., Integration of space-borne and air-borne data in monitoring river ice processes in the Slave River, Canada. Remote Sensing of Environment, 181, 65-81, doi.org/10.1016/j.rse.2016.03.041, 2016.

Cooley, S. W. and T.M. Pavelsky, Spatial and temporal patterns in Arctic river ice breakup revealed by automated ice detection from MODIS imagery. Remote Sens. Environ. 175, 310–322, doi.org/10.1016/j.rse.2016.01.004, 2016.

Duguay, C.R., M. Bernier, Y. Gauthier, and A. Kouraev, Remote sensing of lake and river ice. In Remote Sensing of the Cryosphere, Edited by M. Tedesco. Wiley-Blackwell (Oxford, UK), 273-306, ISBN-13:978-1118368855, 2015.

Duguay, C.R., T.J. Pultz, P.M. Lafleur, and D. Drai, RADARSAT backscatter characteristics of ice growing on shallow sub-arctic lakes, Churchill, Manitoba, Canada. Hydrological Processes, 16(8): 1631-1644, DOI: 10.1002/hyp.1026, 2002.

Ettema R. Review of alluvial-channel responses to river ice. Journal of Cold Regions Engineering 16: 191–217, doi.org/10.1061/(ASCE)0887-381X(2002)16:4(191), 2002.

Gunn G. E., C. R. Duguay, L. C. Brown, J. M. L. King, D. Atwood, and A. Kasurak, Freshwater lake ice thickness derived using surface-based X- and Ku-band FMCW scatterometers, Cold Regions Science and Technology,120, 115–126, doi.org/10.1016/j.coldregions.2015.09.012, 2015.

Gunn G.E., Duguay C.R., Atwood D.K., King J., Toose P., Observing Scattering Mechanisms of Bubbled Freshwater Lake Ice Using Polarimetric RADARSAT-2 (C-Band) and UW-Scat (X- and Ku-Bands), IEEE Transactions on Geoscience and Remote Sensing, 56, 5, doi: 10.1109/TGRS.2017.2786158. ,2018.

Instructions on safety organisation of rivers' and lakes' crossing, RD 34.03.221, INFORMENRGO, Moscow, 1969.

Kang K.-K., C.R. Duguay, J. Lemmetyinen, Y. Gel, Estimation of ice thickness on large northern lakes from AMSR-E brightness temperature measurements, Remote Sensing of Environment, Volume 150, Pages 1-19, doi.org/10.1016/j.rse.2014.04.016, 2014.

Kheyrollah Pour, H., C.R. Duguay, A. Scott, and K.-K. Kang, Improvement of lake ice thickness retrieval from MODIS satellite data using a thermodynamic model. IEEE Transactions on Geoscience and Remote Sensing, 55(10): 5956-5965, doi: 10.1109/TGRS.2017.2718533, 2017.

King, J.M.L., R. Kelly, A. Kasurak, C. Duguay, G. Gunn, and J.B. Mead, UW-Scat - ground-based dual frequency scatterometry for observation of snow processes. IEEE Geoscience and Remote Sensing Letters, 10(3): 528-532, doi: 10.1109/LGRS.2012.2212177, 2013.

King, J., R. Kelly, A. Kasurak, C. Duguay, G. Gunn, N. Rutter, T. Watts, and C. Derksen, Spatio-temporal influence of tundra snow properties on Ku-band (17.2 GHz) backscatter. Journal of Glaciology, 61(226): 267-279, doi: 10.3189/2015JoG14J020, 2015.

Kouraev. A.V., Zakharova. E.A., Samain. O., Mognard. N.M., Cazenave. A., Ob' River discharge from TOPEX/Poseidon satellite altimetry (1992–2002). Remote Sensing of Environment, 93 (1). 238–245, doi.org/10.1016/j.rse.2004.07.007, 2005.

Kouraev A.V., Zakharova E.A., Rémy F., Suknev A.Y. Study of Lake Baikal ice cover from radar altimetry and in situ observations. Marine Geodesy, Special issue on SARAL/AltiKa, 38 (sup1), 477-486, doi.org/10.1080/01490419.2015.1008155, 2015.

Kouraev A.V., Semovski S.V., Shimaraev M., Mognard N.M., Légresy B. , Rémy F., Observations of Lake Baikal ice from satellite altimetry and radiometry, Remote Sensing of Environment, 108, 240–253, doi.org/10.1016/j.rse.2006.11.010, 2007.

Kourzeneva E., Assimilation of lake water surface temperature observations using an extended Kalman filter, Tellus A: Dynamic Meteorology and Oceanography, 66:1, doi:10.3402/tellusa.v66.21510, 2014.

Legrésy, B., & Rémy, F., Surface characteristics of the Antarctic ice sheet and altimetric observations. Journal of Glaciology, 43(14), 265−275, doi.org/10.3189/S002214300000321X, 1997.

Mermoz S., S. Allain, M. Bernier and E. Pottier, Investigation of Radarsat-2 and Terrasar-X data for river ice classification, IEEE International Geoscience and Remote Sensing Symposium, Cape Town, II-29-II-32, doi: 10.1109/IGARSS.2009.5417991, 2009.

Mermoz S., S. Allain-Bailhache, M. Bernier, E. Pottier, J. J. Van Der Sanden and K. Chokmani, Retrieval of River Ice Thickness From C-Band PolSAR Data, in IEEE Transactions on Geoscience and Remote Sensing, 52, 6, 3052-3062, doi: 10.1109/TGRS.2013.2269014, 2014.

Michailovsky, C. I., S. McEnnis, P. A. M. Berry, R. Smith, and P. Bauer-Gottwein, River monitoring from satellite radar altimetry in the Zambezi river basin, Hydrol. Earth Syst. Sci., 16(7), 2181–2192, doi:10.5194/hess-16-2181-2012, 2012.

Morse B., Hicks F., Advances in river ice hydrology 1999–2003, Hydrological Processes, 19, 247–263, doi: 10.1002/hyp.5768, 2005.

Muhammad, P., Duguay, C.R., Kang, K.-K., Monitoring ice break-up on the Mackenzie River using remote sensing. The Cryosphere, 10: 569-584, doi:10.5194/tc-10-569-2016, 2016.

Nilsson, J., Vallelonga, P., Simonsen, S.B., Sorensen, L.S., Forsberg, R., Dahl-Jensen, D., Hirabayashi, M., Goto-Azuma, K., Hvidberg, C.S., Kjaer, H.A., Satow, K., Greenland 2012 melt event effects on CryoSat-2 radar altimetry. Geophys. Res. Lett. 42, 3919–3926, doi: 10.1002/2015GL063296, 2015.

Picard R. and Cook R. Cross-validation of regression models, Journal of the American Statistical Association, 79, 575–583, doi.org/10.2307/2288403, 1984.

Pavelsky, T. M., & Smith, L. C., Spatial and temporal patterns in Arctic river ice breakup observed with MODIS and AVHRR time series. Remote Sensing of Environment, 93, 328–338, doi:10.1016/j.rse.2004.07.018, 2004.

Prowse TD., River-ice ecology: part B. Biological aspects. Journal of Cold Regions Engineering 15: 17–33, doi.org/10.1061/(ASCE)0887-381X(2001)15:1(17), 2001.

Prowse T., Alfredsen K., Beltaos S., Bonsal B., Duguay C., Korhola A., McNamara J., Pienitz R., Vincent W.F., Vuglinskyn V., Weyhenmeyer G.A., Past and Future Changes in Arctic Lake and River Ice. AMBIO, 40:53–62, doi: 10.1007/s13280-011-0216-7, 2011a.

Prowse T., Alfredsen K., Beltaos S., Bonsal B., Bowden W., Duguay C., Korhola A., McNamara J., Vincent W.F., Vuglinskyn V., Anthony K., Weyhenmeyer G.A, Effects of Changes in Arctic Lake and River Ice. AMBIO 40, 63–74,. https://doi.org/10.1007/s13280-011-0217-6, 2011b.

Slater T., A. Shepherd, M. Mcmillan, T. W. K. Armitage, I. Otosaka and R. J. Arthern, Compensating Changes in the Penetration Depth of Pulse-Limited Radar Altimetry Over the Greenland Ice Sheet, IEEE Transactions on Geoscience and Remote Sensing, 57, 12, 9633-9642, doi: 10.1109/TGRS.2019.2928232, 2019.

Unterschultz, K., Van der Sanden, J., Hicks, F., Potential of RADARSAT-1 for the monitoring of river ice: Results of a case study on the Athabasca River at Fort McMurray, Canada. Cold Regions Science and Technology, 55, 238–248, doi:10.1016/j.coldregions.2008.02.003, 2009.

Willatt, R., Laxon, S., Giles, K., Cullen, R., Haas, C., & Helm, V., Ku-band radar penetration into snow cover on Arctic sea ice using airborne data. Annals of Glaciology, 52(57), 197–205, doi.org/10.3189/172756411795931589 2011.

Zakharova, E.A., Kouraev, A.V., Rémy, F., Zemtsov, V.A., Kirpotin, S.N., Seasonal variability of the Western Siberia wetlands from satellite radar altimetry. J. Hydrology, 512, 366–378. doi.org/10.1016/j.jhydrol.2014.03.002, 2014.

Zakharova E.A., I.N. Krylenko, A.V. Kouraev, Use of non-polar orbiting satellite radar altimeters of the Jason series for estimation of river input to the Arctic Ocean, Journal of Hydrology, 568, 322-333, doi.org/10.1016/j.jhydrol.2018.10.068, 2019.

Zakharova EA., Nielsen K., Kamenev G., Kouraev A., River discharge estimation from radar altimetry: Assessment of satellite performance, river scales and methods. Journal of Hydrology, 583, 124561, doi.org/10.1016/j.jhydrol.2020.124561, 2020.